

Supplement of Atmos. Meas. Tech., 11, 2325–2343, 2018
<https://doi.org/10.5194/amt-11-2325-2018-supplement>
© Author(s) 2018. This work is distributed under
the Creative Commons Attribution 4.0 License.



Supplement of

Laser ablation aerosol particle time-of-flight mass spectrometer (LAAPTOF): performance, reference spectra and classification of atmospheric samples

Xiaoli Shen et al.

Correspondence to: Harald Saathoff (harald.saathoff@kit.edu)

The copyright of individual parts of the supplement might differ from the CC BY 4.0 License.

1 In the supporting information, the contents are organised as 1) tables, 2) figures, and 3) description of some procedures for
 2 LAAPTOF data analysis as well as the corresponding equations and uncertainties.

3

4 **Table S1: Summary of peak assignments**

Cations				Anions			
m/z	carbon	inorganic	organic	m/z	carbon	inorganic	organic
7+		Li ⁺		1-		H ⁻	
12+	C ⁺			8-		O ²⁻	
13+			CH ⁺	12-	C ⁻		
15+			CH ₃ ⁺ /NH ⁺	16-		O ⁻	
17+		OH ⁺		17-		OH ⁻	
18+		NH ₄ ⁺ /H ₂ O ⁺		24-	C ₂ ⁻		
23+		Na ⁺		25-			C ₂ H ⁻
24+	C ₂ ⁺	Mg ⁺		26-			CN/C ₂ H ₂ ⁻
27+		Al ⁺	C ₂ H ₃ ⁺	32-		S ⁻	
28+		Si ⁺	CO ⁺	36-	C ₃ ⁻		
29+			C ₂ H ₅ ⁺ /CHO ⁺	35-		Cl ⁻	
30+		NO ⁺	CH ₃ NH ⁺ /CH ₂ O ⁺	37-		Cl ⁻	
36+	C ₃ ⁺			42-			CNO/C ₂ H ₂ O ⁻
39+		K ⁺	C ₃ H ₃ ⁺	43-		AlO ⁻	
40+		Ca ⁺	C ₂ O ⁺	45-			COOH ⁻
41+		K ⁺	C ₃ H ₅ ⁺	46-		NO ₂ ⁻	
43+			C ₃ H ₇ ⁺ /C ₂ H ₃ O ⁺	48-	C ₄ ⁻	SO ⁻	
44+		SiO ⁺	CO ₂ ⁺	59-		AlO ₂ ⁻	CH ₂ COOH ⁻
46+		NO ₂ ⁺		60-	C ₅ ⁻	SiO ₂ ⁻	
48+	C ₄ ⁺			62-		NO ₃ ⁻	
51+			C ₄ H ₃ ⁺	63-		PO ₂ ⁻	
53+			C ₄ H ₅ ⁺	64-		SO ₂ ⁻	
54+		Fe ⁺		70-		³⁵ Cl ₂ ⁻	
55+		Mn ⁺	C ₄ H ₇ ⁺ /C ₃ H ₃ O ⁺	71-			CCH ₂ COOH ⁻
56+		Fe/CaO/Si ₂ ⁺	C ₄ H ₈ ⁺	72-	C ₆ ⁻	FeO ⁻	
57+		CaOH ⁺	C ₄ H ₉ ⁺ /C ₂ OOH ⁺	73-			C ₂ H ₄ COOH ⁻
58+		Ni ⁺	C ₂ H ₅ -NH-CH ₂ ⁺	76-		SiO ₃ ⁻	
59+			(CH ₃) ₃ N ⁺	77-		HSiO ₃ ⁻	
60+	C ₅ ⁺			79-		PO ₃ ⁻	
63+		Cu ⁺	C ₅ H ₃ ⁺	80-		SO ₃ ⁻	
64+		Zn ⁺		81-		HSO ₃ ⁻	
65+		Cu ⁺		84-	C ₇ ⁻		
66+		Zn ⁺		85-			C ₃ H ₄ COOH ⁻
69+			C ₅ H ₉ ⁺	86-		FeO ₂ ⁻	
71+			C ₄ H ₇ O ⁺	88-		Si ₂ O ₂ ⁻ /FeO ₂ ⁻	
72+	C ₆ ⁺			89-			(CO) ₂ OOH ⁻
77+			C ₆ H ₅ ⁺	93-		NaCl ₂ ⁻	
81+		Na ₂ Cl ⁺	C ₆ H ₉ ⁺	95-		NaCl ₂ ⁻ /PO ₄ ⁻	
83+		Na ₂ Cl ⁺	C ₅ H ₇ O ⁺	96-	C ₈ ⁻	SO ₄ ⁻	
84+	C ₇ ⁺			97-		HSO ₄ ⁻	
85+			C ₇ H ₅ ⁺ /C ₃ HO ₃ ⁺	99-			C ₄ H ₆ COOH ⁻
88+		FeO ₂ ⁺		103-		(AlO)SiO ₂ ⁻	
91+			C ₇ H ₇ ⁺	108-	C ₉ ⁻		
95+			C ₇ H ₁₁ ⁺	109-		KCl ₂ ⁻	
96+	C ₈ ⁺	Ca ₂ O ⁺		117-			(CO) ₃ OOH ⁻
97+		KNaCl ⁺	C ₄ HO ₃ ⁺	119-		AlSiO ₄ ⁻ /NaSO ₄ ⁻	
103+			C ₈ H ₇ ⁺	130-		NaCl ₃ ⁻	
105+			C ₈ H ₉ ⁺	135-		KSO ₄ ⁻	
108+	C ₉ ⁺			136-		(SiO ₂) ₂ O ⁻ /KHSO ₄ ⁻	
112+		(CaO) ₂ ⁺		148-		(SiO ₂) ₂ Si ⁻	
113+		K ₂ Cl ⁺		151-		Na ₂ Cl ₃ ⁻	
115+		K ₂ Cl ⁺	C ₉ H ₇ ⁺	153-		Na ₂ Cl ₃ ⁻	
120+	C ₁₀			179-		AlSiO ₄ .SiO ₂ ⁻	
132+	C ₁₁ ⁺						
206-208+		Pb ⁺					

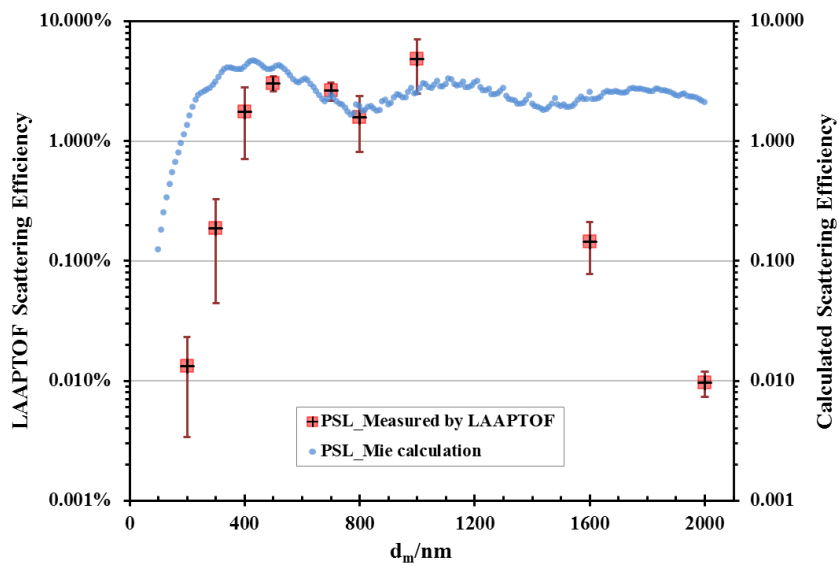
5

6 **Table S2: Codes for reference particle types used for classification by using the reference spectra based classification**

positive code	reference particle	negative code	reference particle
01	Ammonium Nitrate	01	Ammonium Nitrate and Sulfate
02	Pinonic Acid	02	Ammonium Nitrate and Potassium Sulfate
03	Oxalic Acid	03	Desert Dust (Morroco)
04	Ammonium Nitrate and Potassium Sulfate	04	Urban Dust
05	Potassium Sulfate Coated PSL	05	Arable Soil Dust (German) (SDGe01)
06	Agricultural Soil Dust	06	Diesel Soot
07	Diesel Soot	07	Biomass Burning Soot
08	Biomass Burning Soot		
09	Sea salt (pure)		
10	Fuzzy Class 6_Calcium rich		

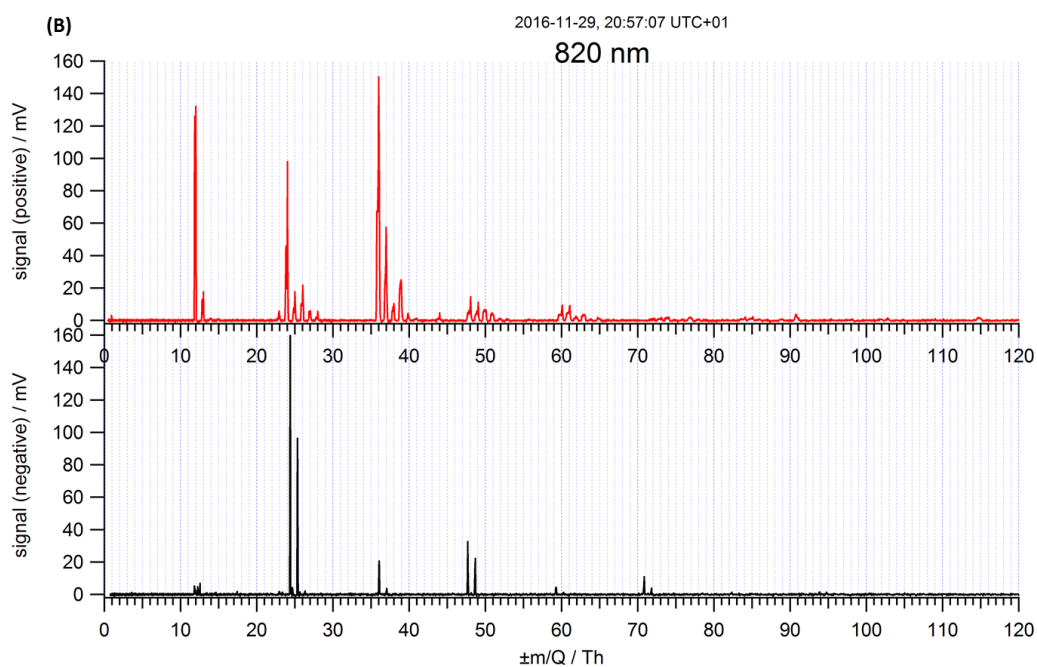
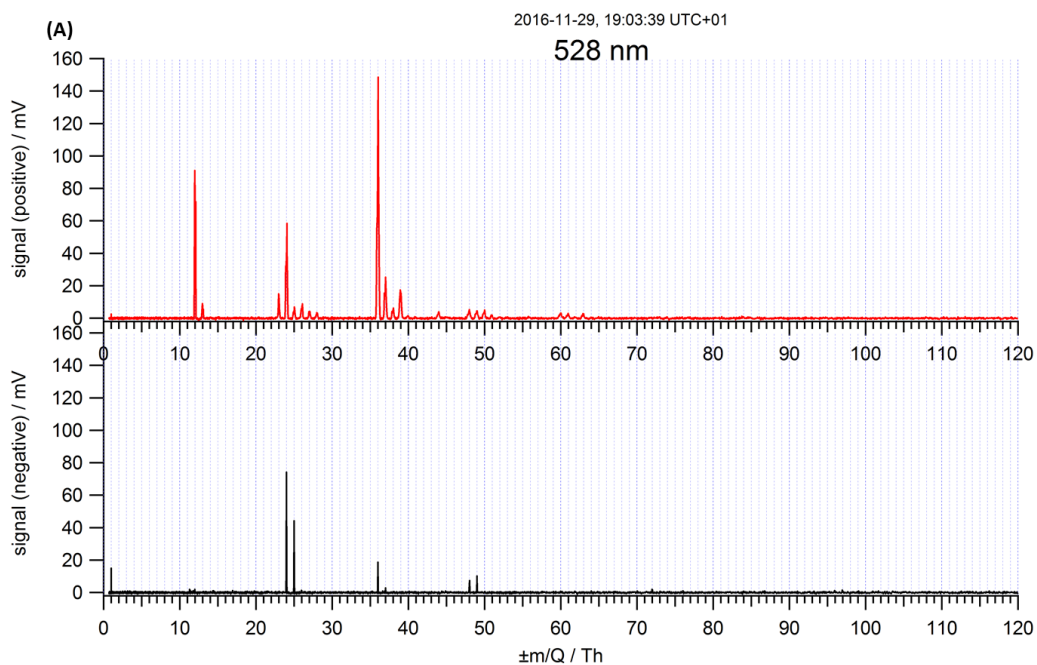
7

8 Note: In order to minimize the complexity, the reference number was reduced by observing the histogram of particle types based on the
 9 correlation between each ambient spectrum (7314 in total) and our 32 laboratory based reference spectra relevant for atmospheric aerosol
 10 (refer to the details of reference spectra based classification in Procedures 2 in the supplementary information).



11

12 Figure S1: Comparison of scattering efficiencies for PSL particles measured by LAAPTOF and values from Mie calculation at the
 13 particle sizes relevant to measurement. The input parameters for Mie calculation are refractive index of 1.62 and wavelength of
 14 405 nm.

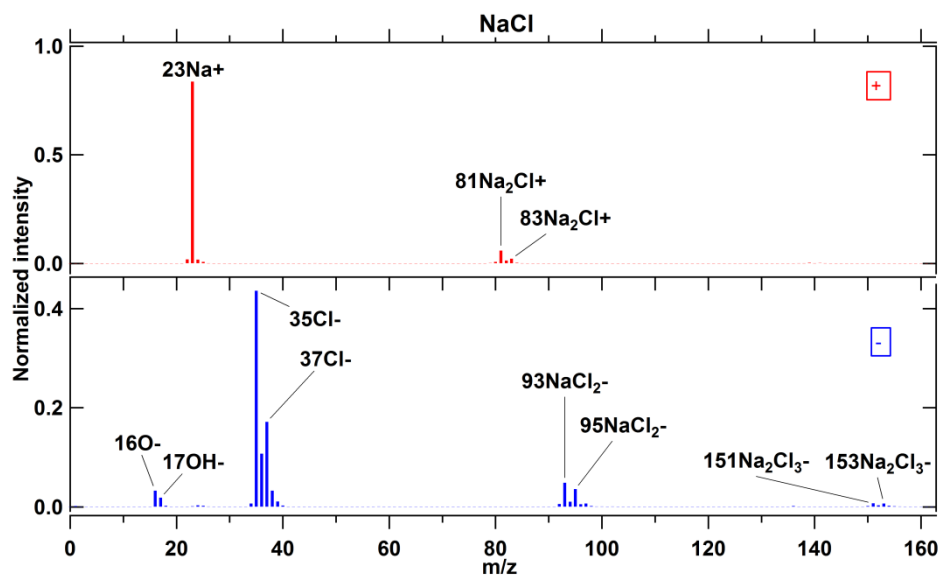


15

16

17

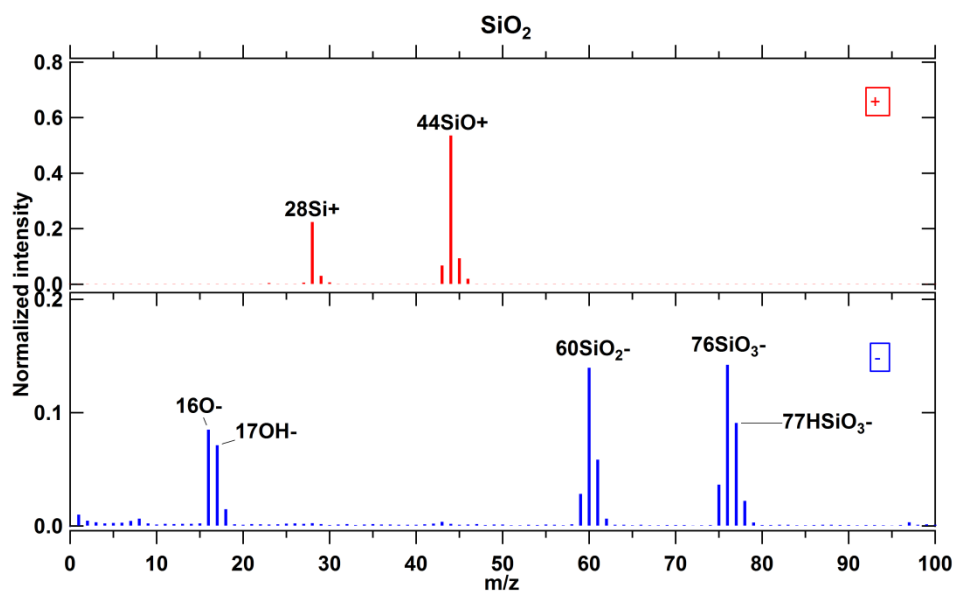
Figure S2: Typical spectra with raw signal for individual PSL particles of dva 528 nm (panel A) and 820 nm (panel B), respectively.



18

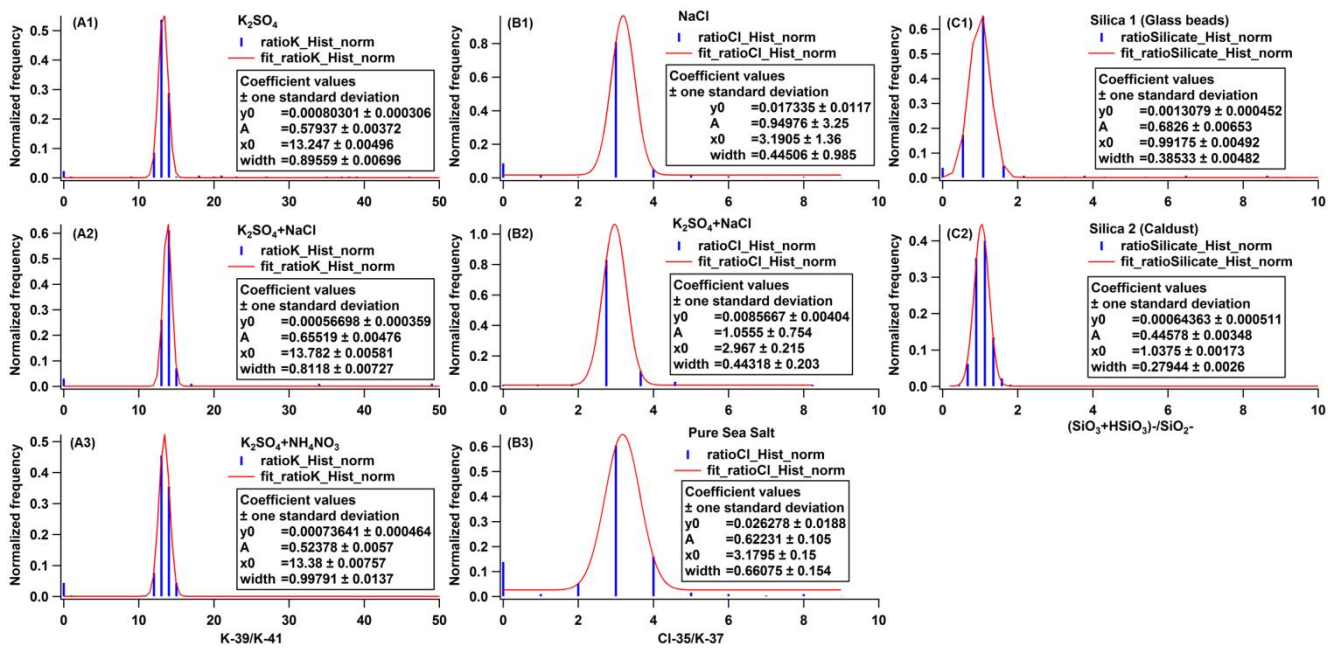
19 Figure S3: Average mass spectrum for 1170 nm (d_{va}) pure NaCl particles. The ratio of m/z 35 Cl⁻ to m/z 37 Cl⁻ is ~ 3.2 , similar as
 20 the natural isotopic ratio of ~ 3.1 for $^{35}\text{Cl}/^{37}\text{Cl}$. 250 single particle mass spectra were averaged for this spectrum.

21



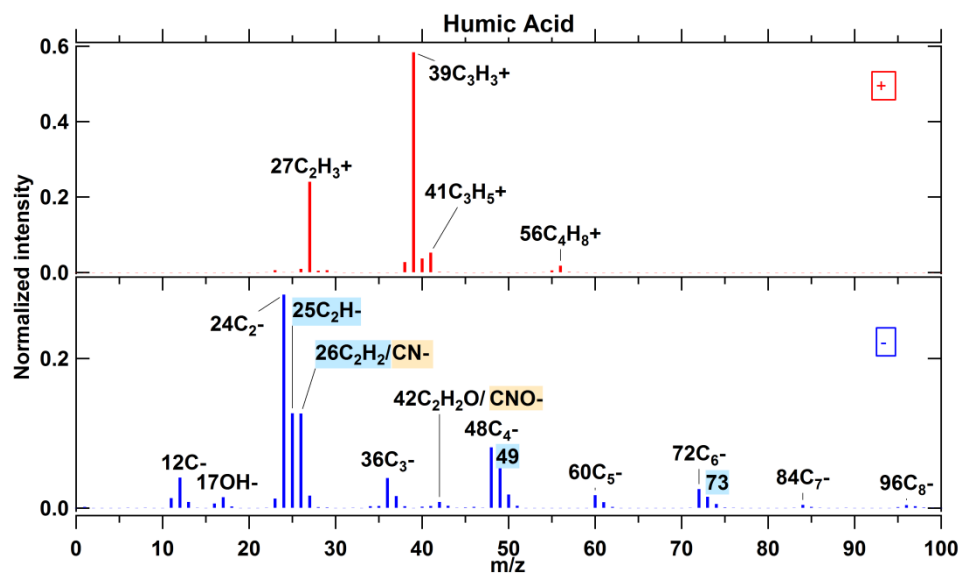
22

23 Figure S4: Average mass spectrum for 2097 nm (d_{va}) SiO₂ particles (glass beads). The ratio of m/z 44 SiO⁺ to m/z 28 Si⁺ is ~ 2.4 ;
 24 (m/z 76 SiO₃⁻ + m/z 77 HSiO₃⁻) to m/z 60 SiO₂⁻ is ~ 1 . Such peak ratios are typical for SiO₂ particles. 347 single particle mass
 25 spectra were averaged for this spectrum.



27

28 Figure S5: Histogram of peak ratios for different particle samples: panel A1 to A3 are for the isotopic ratio of K-39/K-41 arising
 29 from K containing samples; panel B1 to B3 are for the isotopic ratio of Cl-35/Cl-37 arising from Cl containing samples; panel C1
 30 and C2 are for the peak ratio of $(SiO_3+HSiO_3^-)/SiO_2^-$ arising from silicate containing samples.

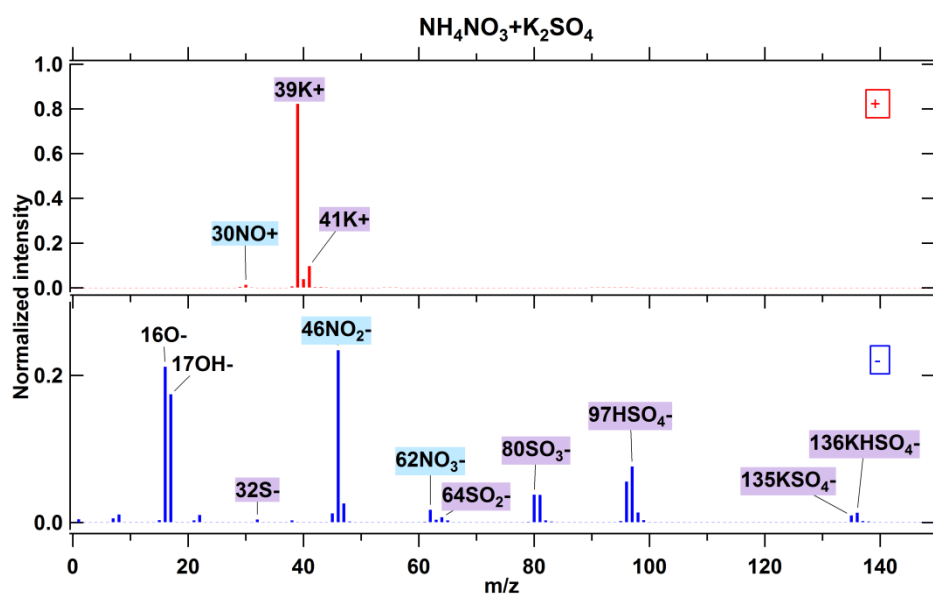


31

32 Figure S6: Average mass spectrum for 1221 nm (d_{va}) humic acid particles. Fragments labelled in blue are typical for unsaturated
 33 organic compounds; fragments labelled in orange are from nitrogen-containing organic compounds. 773 single particle mass
 34 spectra were averaged for this spectrum.

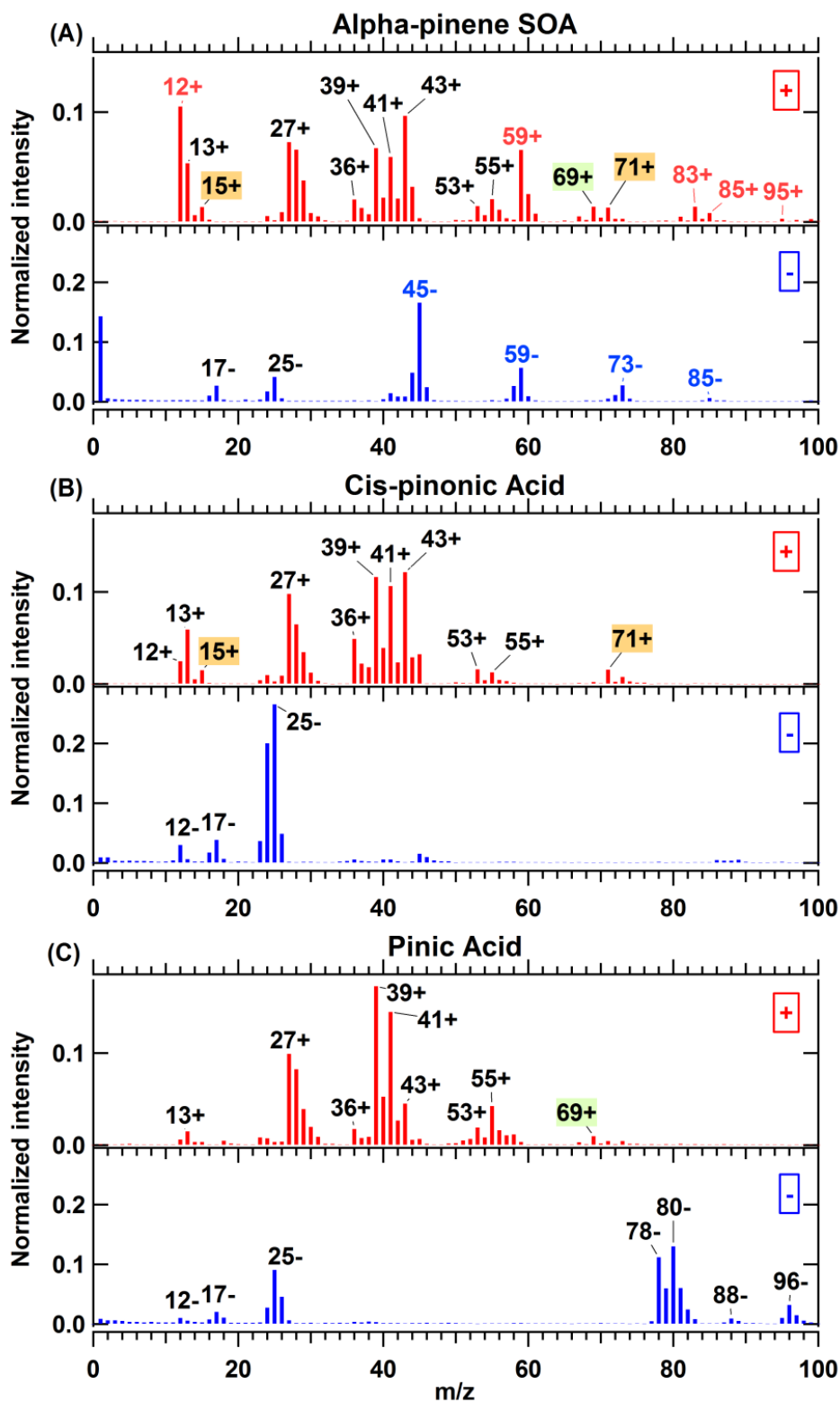
35

36



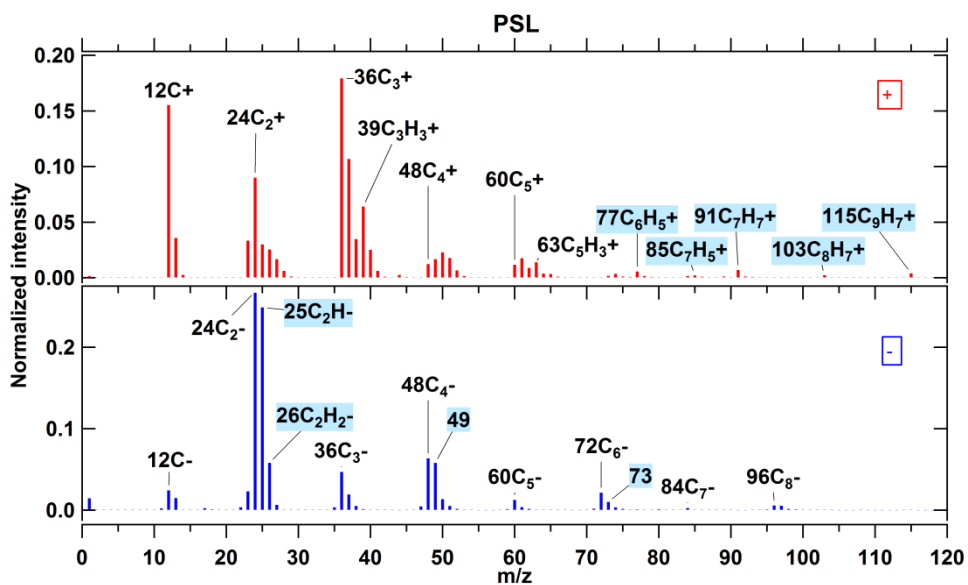
37

38 Figure S7: Average mass spectrum for 854 nm (d_{va}) particles of homogeneous internal mixtures of inorganic compounds, NH_4NO_3
 39 and K_2SO_4 , 576 single spectra averaged. The blue and purple labels represent the fragments arising from pure NH_4NO_3 and pure
 40 K_2SO_4 components, respectively.



41

42 Figure S8: Average mass spectra for particles of homogeneous internal mixtures of (A) secondary organic aerosol (SOA) particles
 43 from α -pinene ozonolysis, which was performed in the APC chamber then the resulting particles were transferred into AIDA
 44 chamber at 263 K and 95% RH, d_{va} = 505 nm, 1938 single spectra averaged, as well as pure aerosol particles consisting of (B) cis-
 45 pinonic acid, d_{va} = 702 nm, 600 single spectra averaged and (C) pinic acid, d_{va} = 902 nm, 683 single spectra averaged. In panel (A),
 46 m/z 15⁺ and 71⁺ labelled in orange are arising from cis-pinonic acid, while m/z 69⁺ labelled in green is arising from pinic acid.

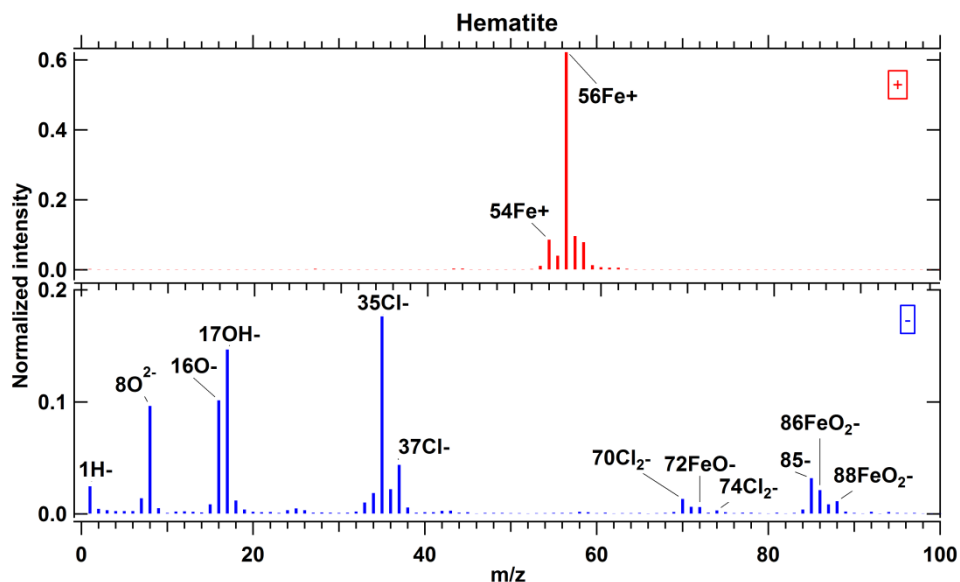


47

48 **Figure S9: Average mass spectra for 818 nm (d_{va}) pure PSL. Fragments labelled in blue are typical patterns for aromatic**
 49 **compounds. 235 single particle mass spectra were averaged for this spectrum.**

50

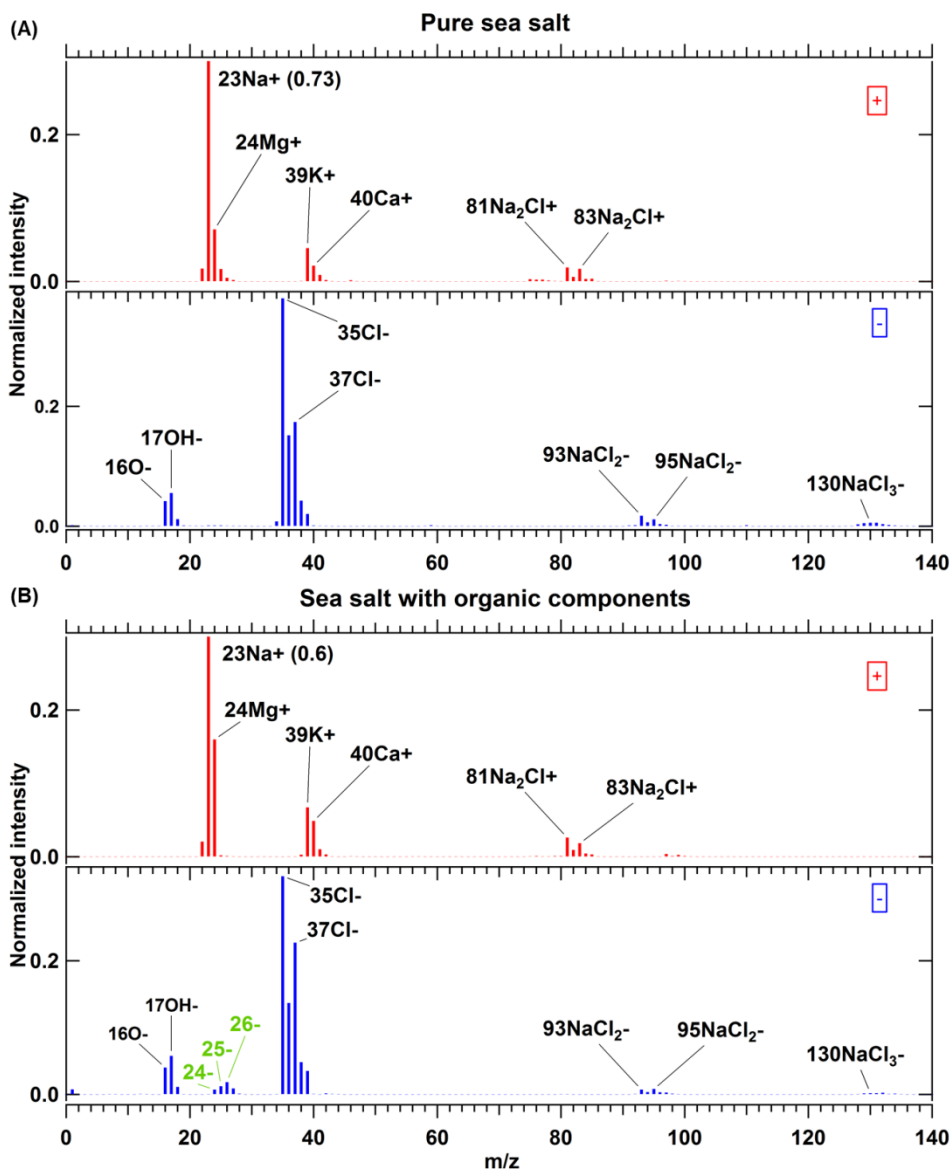
51



52

53 **Figure S10: Average mass spectrum for 800 nm (geometric size) hematite particles, 320 single spectra averaged.**

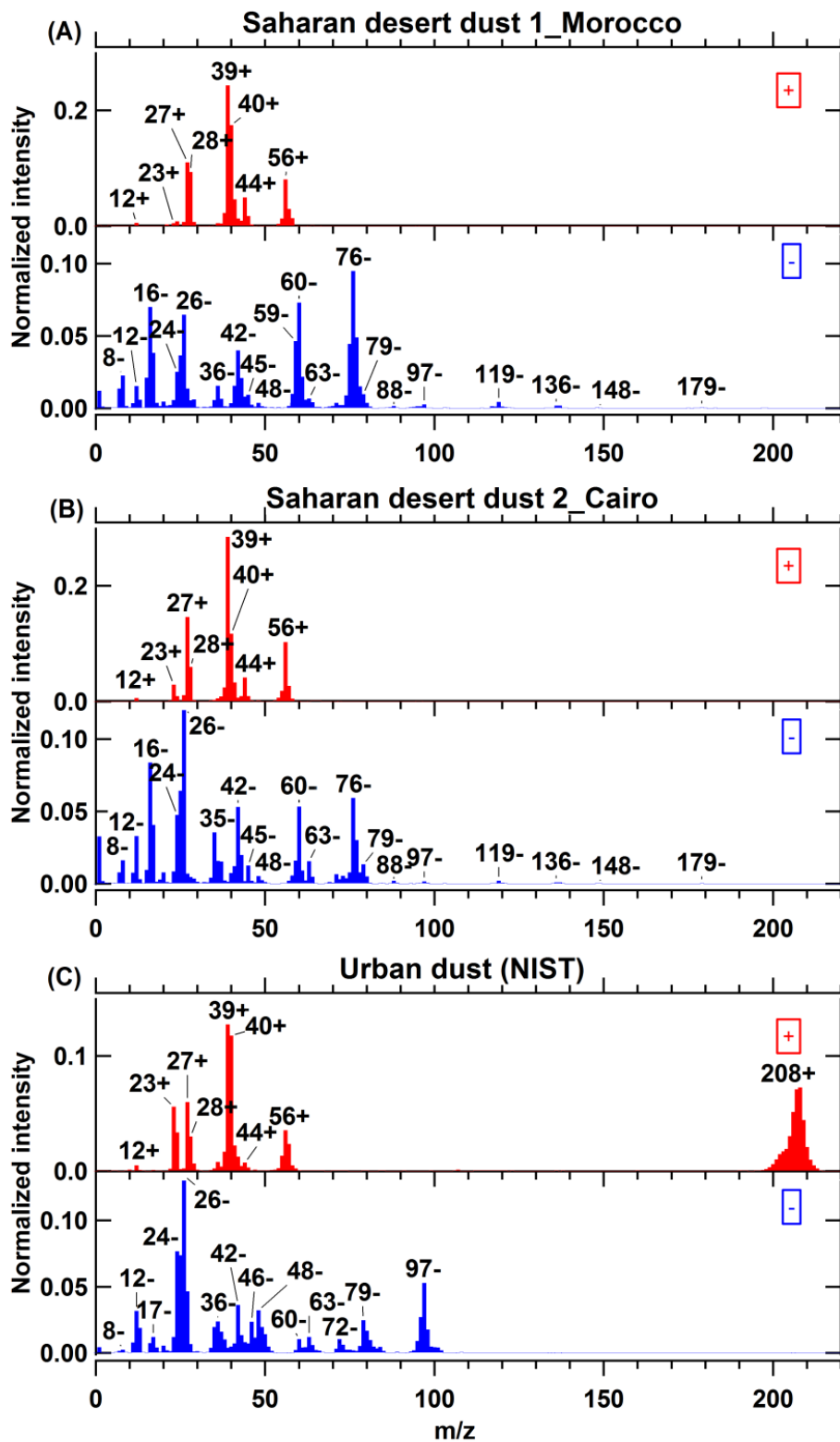
54 Hematite with signatures for iron (intensive m/z 56 Fe^+ and the other iron isotopes m/z 54, 57, and 58), oxides of iron
 55 (m/z 72 FeO^- , 86 FeO_2^- , and 88 FeO_2^-), and chlorides (m/z 35 Cl^- , 37 Cl^- , 70 Cl_2^- , and 74 Cl_2^-). Chloride ions observed
 56 originate from the hematite synthesis process. This is comparable to the hematite spectra measured by PALMS (Gallavardin
 57 et al., 2008).



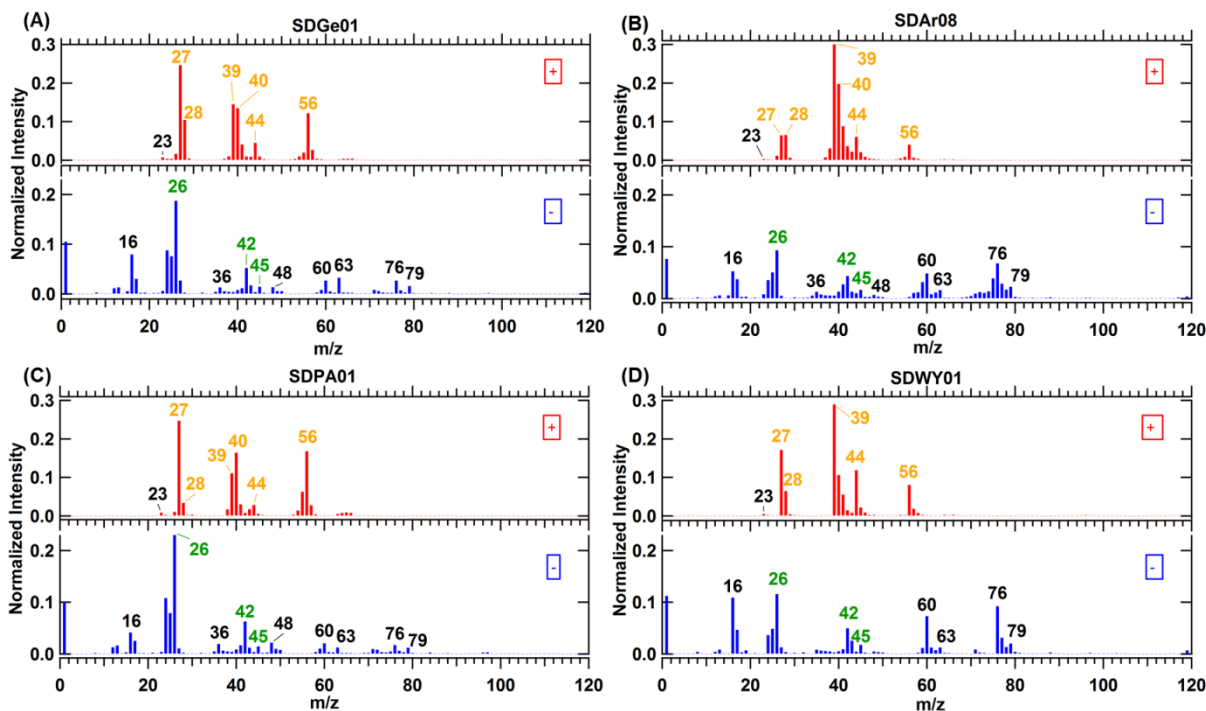
58

59 **Figure S11: Average mass spectra for (A) pure sea salt, 422 single spectra averaged, and (B) sea salt particles with *skeletonema***
 60 ***marinoi* (organic components), 526 single spectra averaged. These aerosol particles were sampled from the AIDA chamber at 246**
 61 **K and 75% RH, $d_{va} = \sim 1200$ nm. The numbers in brackets beside peaks 23^+ are the exact intensity values for them. In panel (B)**
 62 **obvious organic signatures m/z 24⁻, 25⁻, and 26⁻ labelled in green can be observed.**

63 Pure sea salt particles have signatures for NaCl (m/z 23⁺, 81⁺, 83⁺, 35⁻, 37⁻, 93⁻, and 95⁻), and other metals (m/z 24 Mg⁺,
 64 39 K⁺, and 40 Ca⁺). Sea salt particles containing biological components have the signatures for pure sea salt as well as the
 65 signatures for organic compounds (m/z 24⁻, 25⁻, and 26⁻).



66
 67 Figure S12: Average mass spectra for Saharan desert dust from (A) Morocco, 338 single spectra averaged and (B) Cairo city, 396
 68 single spectra averaged, and (C) urban dust (standard material from NIST), 375 single spectra averaged.

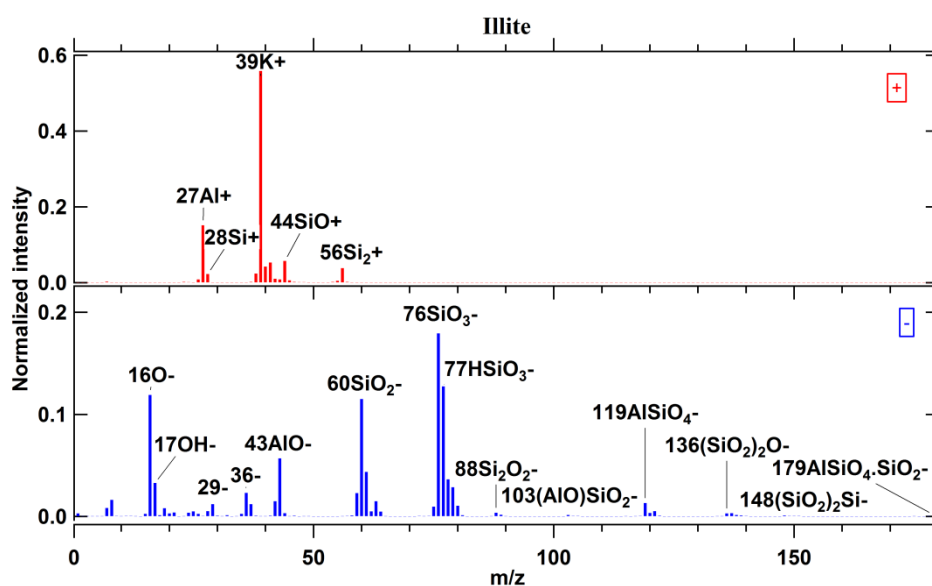


69

70 Figure S13: Average mass spectra for four different arable soil dusts sampled at two sites from Germany (SDGe01 is from
 71 Gottesgabe and SDPA01 is from Paulinenaue), Argentina (SDAr08), and Wyoming in USA (SDWY01). The corresponding aerosol
 72 particles were dispersed by a rotating brush generator and injected via cyclones into the AIDA chamber at 256 K and 80% RH.
 73 Black tags represent inorganic fragments; green tags represent organic fragments; orange tags represent fragments originating
 74 from inorganic and organic species. The numbers of spectra for each average spectrum are 583 (A), 592 (B), 385 (C) and 623 (D).

75

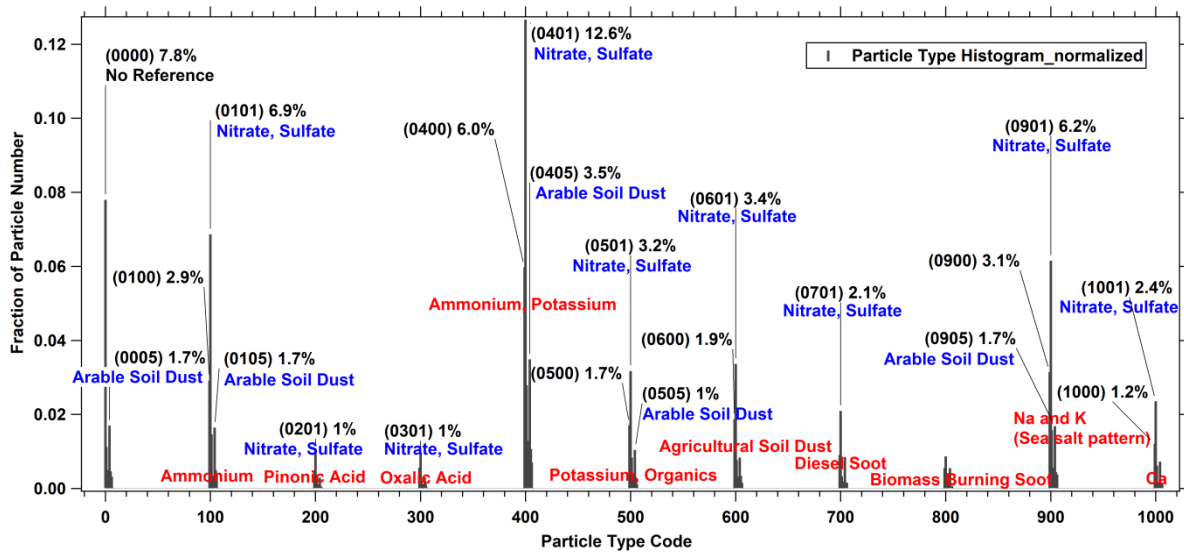
76



77

78 Figure S14: Average mass spectra for illite particles, 807 single spectra averaged

79 Illite particles, mainly containing aluminosilicates, showed signatures for potassium (m/z 39 K^+ and 41 K^+), alumina (m/z
 80 27 Al^+ , 43 AlO^- , and 59 AlO_2^-), silica (m/z 28 Si^+ , 44 SiO^+ , 56 Si_2^+ , 60 SiO_2^- , 76 SiO_3^- , 77 $HSiO_3^-$, 136 $(SiO_2)_2O^-$, and 148
 81 $(SiO_2)_2Si^-$), and oxides of aluminium and silicon (m/z 119 $AlSiO_4^-$, and 179 $AlSiO_4.SiO_2^-$). The K/Si ratio is ~ 25 , which is
 82 comparable to this ratio observed in Illite spectra measured by PALMS (Zawadowicz et al., 2017).



83

84 Figure S15: Particle type histogram based on the classification of field data (on July 29th, 2016 during TRAM01 campaign)
 85 according to laboratory-based reference spectra. The numbers in the brackets are the combination of positive (the front two digits)
 86 and negative codes (the rear two digits) for reference particles, which are listed in Table S2. There are 11 clusters in this plot with
 87 10 positive references labelled in red texts, while the corresponding negative references are labelled in blue texts beneath the
 88 corresponding codes.

89

90 **Procedure 1: LAAPTOF data analysis with emphasize on mass calibration**

91 1. Open two Igor experiments, using the same raw data (One is for comparison, another is for further analysis)
92 2. In one Igor experiment: go through the raw spectra (e.g. from the negative spectra, m/z 1, 16 and 17, 24, 25 and 26 are
93 easier to be recognized), to find out the possible fragments, with the help of peak assignments in Table 1 as well as the
94 laboratory based reference spectra.

95 3. In another Igor experiment
96 • Setting the First-tof, base line, and remove the empty spectra
97 • Start mass calibration

98 Step1: Choose 3 masses with relative bigger distance for positive and negative spectra for basic calibration, respectively.

99 (Tips: it is better to choose the corresponding positions for such masses in the spectrum # -1 after pressing the tab
100 "Display spectrum", which give us the stack spectra showing the shift, thus help us better locate the mass; double
101 check the mass values referring to the other Igor experiment with only raw data)

102 Step2: Exact calibration, by using more masses.

103 (Tips: use only values which are certain)

104 Step3: Generate and check the average spectra, then adjust mass calibration by experience and comparing with the
105 individual spectrum.

106 (Tips: If we have done good mass calibration, the resulting average spectra will be representative, which can help
107 to find more fragments including reasonable patterns like m/z 24⁻, 25⁻, and 26⁻ as well as some expected small
108 fragments like m/z 119⁻ in mineral dust, thus can modify the exact calibration table. Otherwise, we should redo
109 mass calibration from step 1)

110 Step4: Plot ptof vs masses for mass calibration, then use power fit to see whether the value is around 0.5, if yes, then the
111 mass calibration is ok.

112 Step5: If the data is poly dispersed, we can also use fuzzy classification to double check the mass calibration.

113 (Tips: If we have good mass calibration, the fuzzy results will be good, namely the real number of output classes
114 can finally (almost) equal to the input class number)

115 4. Generate average spectra that are normalized to the sum of ion intensities

116 5. Fuzzy Clustering

117 For poly-dispersed particles, we can use Fuzzy classification method. The most important input parameter is the number
118 of classes. We can start from the bigger value (e.g. 20) to the smaller one, until the reasonable number and
119 corresponding classes are found. In this study 6 classes have been found by using this method.

120 (Tips: similar classes would be observed if the input number of classes is too big, and the good situation is that the
121 resulting number of classes we found is equal to the input number, which is 6 in this study. In addition, the resulting number
122 of classes with clearly different features strongly depends on the experience of the operating scientist to identify them.

123 It should be noted that there are spectra-to-spectra peak shifts (~100 ns) due to variance in the position of the interaction
124 of the individual particles with the excimer laser beam, complicating mass calibration. This cannot be corrected with the
125 existing Aeromegt software or the LAAPTOF instrument. It could be avoided by adding/implementing a pulsed extraction,
126 which would store the ions for a certain time and then extract them into the TOF region. Peak shifting is less problematic for
127 the negative spectra than for the positive spectra. This cannot be completely solved even after aforementioned serious mass
128 calibration. Such peak shifting is less problematic in the negative spectra than the positive ones.

129 Procedure 2: Reference spectra based classification

130 Step 1: Normalize (to sum) stick spectra from the field data and reference spectra.

131 Step 2: Correlate each ambient spectrum with each reference spectrum (positive spectra 01 to 32 and negative spectra 01
132 to 32). Positive and negative spectra are treated separately due to differences in peak intensities for the two polarities, biasing
133 coefficients r (refer to equation S1); namely high intensive peaks dominating the value of r . However, this can be reduced by
134 selecting specific mass ranges for the correlation.

135 Step 3: Define particle type. Only correlations with a Pearson's correlation coefficient $r \geq 0.6$ are used. Particles are
136 categorized using a 4-digit code: The first 2 digits identify the positive reference spectrum (01 – 32) with which a particle's
137 spectrum exhibits maximum r ; the third and fourth digits the negative reference spectrum (01 – 32) with which the particle's
138 negative spectrum exhibits maximum r .

139 Step 4: Reduce the number of references. A histogram with the number of particles per particle type is used to identify
140 the main particle types. For positive spectra, particle types with number fractions $\geq 1\%$ were chosen. For the negative
141 spectra, no numerical criteria could be used in the first iteration, but spectra were examined individually (we found e.g. that
142 four arable soil dust samples had similar negative spectra and only used SDGe01). For our dataset the number of reference
143 spectra or particle types was reduced to 10 positive and 7 negative spectra (Table S2).

144 Step 5: Repeat step 1 to 3 using the reduced set of reference spectra.

145 Step 6: Identify the main particle types. Categorized particles are again plotted in a histogram, and main particle types
146 are identified based on number fractions $\geq 1\%$. Only particles with correlations in both polarities are included here. In our
147 study, 13 main types were found.

148 **The equation (S1) for calculating Pearson's correlation coefficients between two waves A and B (e.g. ambient and**
149 **reference spectrum)**

$$150 \quad r = \frac{\sum_{i=0}^{n-1} (\text{waveA}[i] - A)(\text{waveB}[i] - B)}{\sqrt{\sum_{i=0}^{n-1} (\text{waveA}[i] - A)^2 \sum_{i=0}^{n-1} (\text{waveB}[i] - B)^2}} \quad (\text{S1})$$

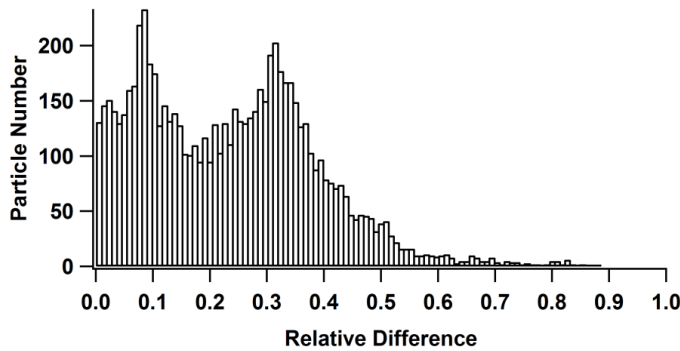
151 Here A is the average of the elements in wave A , B is the average of the elements of wave B and the sum is over all
152 wave elements. Although we mainly discuss the main peaks with higher intensities, in this paper, it is should be mentioned
153 that the bias by the peak intensity in calculating r are inevitable, namely high intensive peaks dominate the value of r . Of
154 course this intensity bias can be reduced by selecting specific mass ranges for the correlation.

155

156 **Uncertainties for reference-oriented method for grouping mass spectra**

157 In order to estimate the uncertainty for reference-oriented method, we have calculated the relative difference between the
 158 highest and the second highest Pearson’s correlation coefficients (r1 and r2) for each particle, according to equation (S2):

159
$$\text{Relative Difference} = \frac{r1-r2}{r1} = \frac{r1_{\text{pos}} \times r1_{\text{neg}} - r2_{\text{pos}} \times r2_{\text{neg}}}{r1_{\text{pos}} \times r1_{\text{neg}}} \quad (\text{S2})$$



160
 161 **Figure S16: Histogram of relative difference between the highest and the second highest Pearson’s correlation coefficient values**
 162 **for each particle measured in the field (on July 29th, 2016 during TRAM01 campaign).**

163 The corresponding statistic calculation results for such relative difference data are listed as follows:

164 V_npnts= 7314; V_numNaNs= 0; V_numINFs= 0; V_avg= 0.234484;

165 V_Sum= 1715.02; V_sdev= 0.152986; V_sem= 0.00178885;

166 V_rms= 0.279972; V_adev= 0.126782; V_skew= 0.595888;

167 V_kurt= 0.244212; V_minloc= 2005; V_maxloc= 5211;

168 V_min= 4.35069e-05; V_max= 0.882732; V_minRowLoc= 2005;

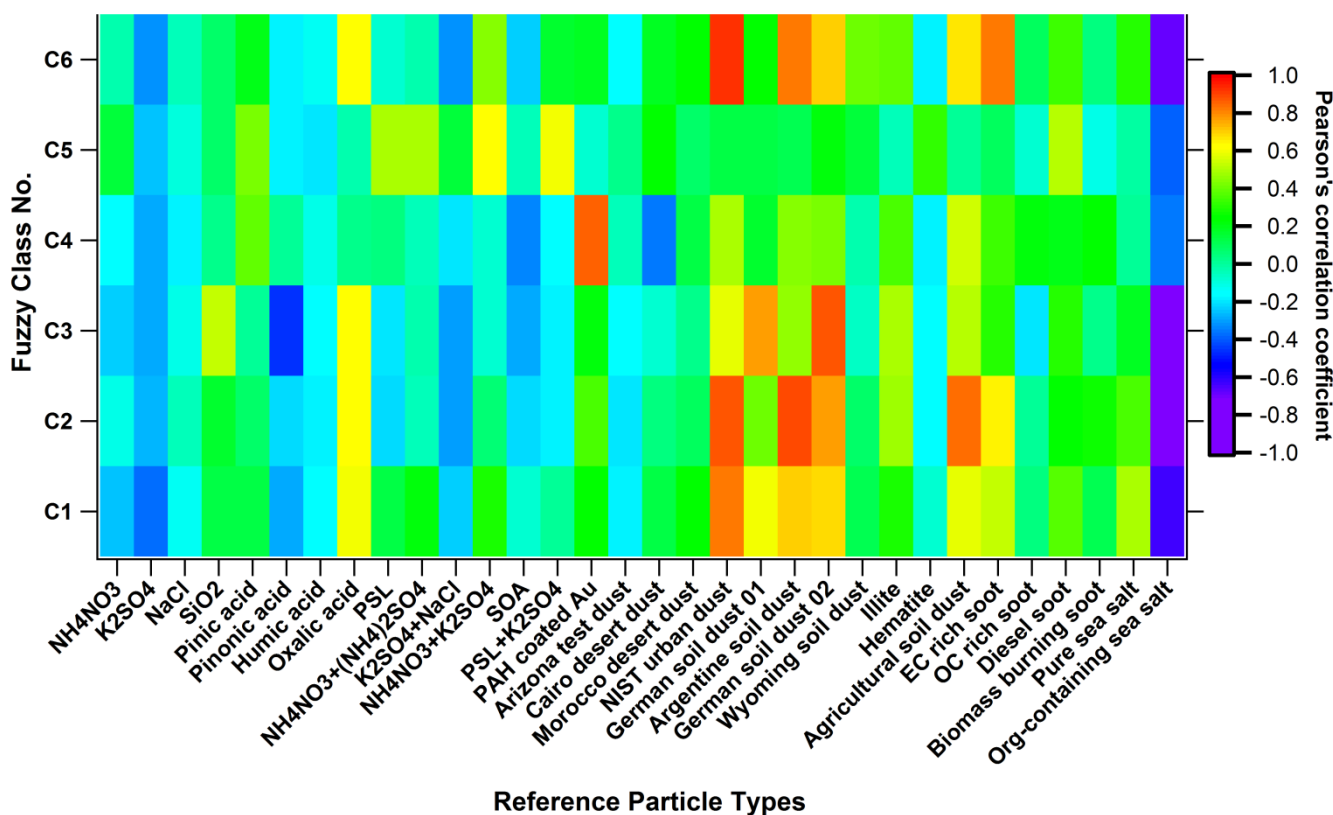
169 V_maxRowLoc= 5211; V_startRow= 0; V_endRow= 7313;

170 The relative difference mentioned above provides information about the uncertainties for using the reference-spectra
 171 oriented method, namely, the bigger the difference is, the smaller the uncertainty will be. It turns out that 77% of the 7314
 172 particles we measured have more than 10% relative difference between r1 and r2, therefore such classification method is
 173 reasonable to be used.

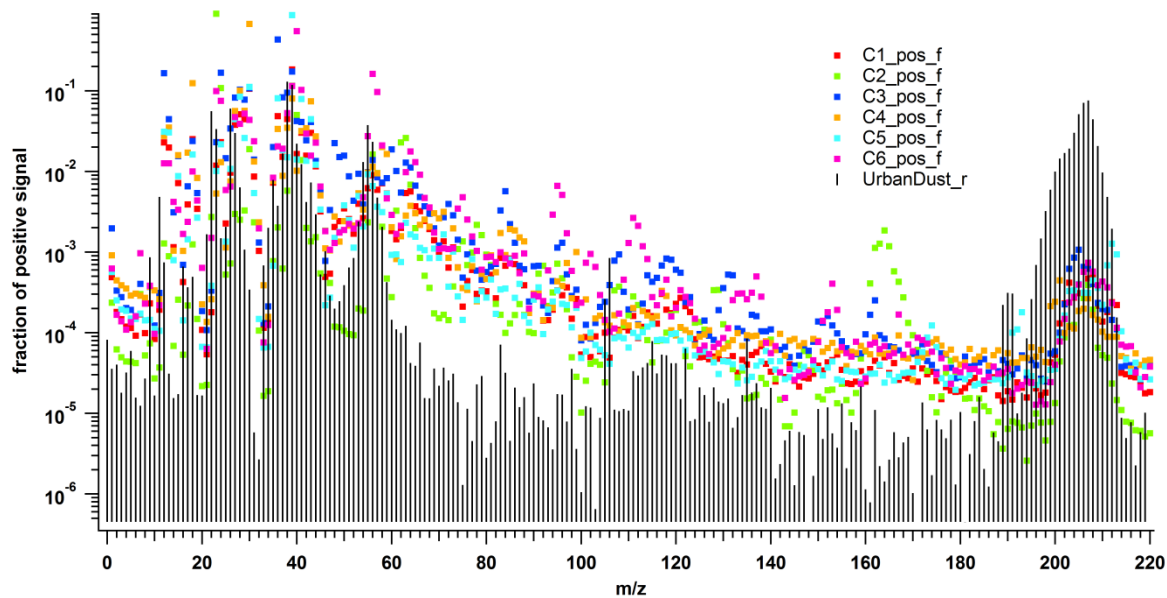
174 There are some factors that could have impact on the uncertainties: 1) the most important one is selection of reference
 175 spectra, since two similar references such German soil dust SDGe01 and SDPA01 will lead to similar r that cause little
 176 relative difference between r1 and r2 corresponds to higher uncertainty. 2) Peak intensities and mass ranges selected will
 177 influence the r values. Bias by peak intensities leads to higher uncertainties whereas well selected mass ranges can also
 178 reduce the uncertainties.

179 **Procedure 3: Seeking lead (Pb) containing particles using the reference spectra**

180 In order to pick out the lead-containing particles, we firstly check the fuzzy results by correlating them to all the reference
 181 spectra in the size range of 200 to 220. As shown in Fig. S17, all the classes except class 5 have significant correlation with
 182 the lead-containing urban dust particles (NIST), which can also be seen in Fig. S18 where the corresponding spectra are
 183 stacked, showing clear comparable data points in the m/z range of 200 to 220. For Class 5, there are some points offset,
 184 leading to lower r, although it also shows similar shape in such m/z range. In the future we will modify our procedure to do
 185 better mass calibration and avoid the offset/error data points to solve such problem. Another problematic issue, which cannot
 186 completely solved at present, is the peak shifting mentioned before, especially for the fragments with bigger mass, such as
 187 lead. This will make data interpretation more difficult. In the next step, we correlate each spectrum with the urban dust
 188 particles in the m/z range of 200 to 220, and the Pb-containing particles can be selected based on the criteria of $r \geq 0.6$. As a
 189 result, 55 Pb-containing particles have been found among 7314 particles in the ambient data. Of course also other specific
 190 particles can be found using suitable reference spectra.
 191



192
 193 **Figure S17: Correlation between fuzzy classification results (6 classes, C1 to C6) and laboratory-based reference spectra only in**
 194 **the m/z range of 200 to 220 for the positive spectra. PAH is short for poly(allylamine hydrochloride), biomass burning soot is the**
 195 **lignocellulosic char from chestnut wood.**



196

197 **Figure S18: Stacked mass spectra for urban dust particles (NIST) and 5 classes of particles measured on July 29th, 2016 during**
 198 **the field campaign TRAM01.**

199

200

201 **References**

202 Gallavardin, S., Lohmann, U., and Cziczo, D.: Analysis and differentiation of mineral dust by single particle laser mass
 203 spectrometry, *Int J Mass Spectrom*, 274, 56–63, 2008.

204 Zawadowicz, M. A., Froyd, K. D., Murphy, D., and Cziczo, D. J.: Improved identification of primary biological aerosol
 205 particles using single particle mass spectrometry, *Atmos Chem Phys*, 17, 7193–7212, 2017.